Numerical simulation of the coalescence-induced polymeric droplet jumping on superhydrophobic surfaces

Kazem Bazesefidpar [a,*], Luca Brandt [a,b], Outi Tammisola [a]

[a] SeRC (Swedish e-Science Research Centre) and FLOW, Dept. of Engineering Mechanics, KTH Royal Institute of Technology, SE-10044 Stockholm, Sweden
[b] Dept. of Energy and Process Engineering, Norwegian University of Science and Technology (NTNU), Trondheim, Norway

ARTICLE INFO

ABSTRACT

Self-propelled jumping of two polymeric droplets on superhydrophobic surfaces is investigated by three-dimensional direct numerical simulations. Two identical droplets of a viscoelastic fluid slide, meet and coalesce on a surface with contact angle 180 degrees. The droplets are modelled by the Giesekus constitutive equation, introducing both viscoelasticity and a shear-thinning effects. The Cahn–Hilliard Phase-Field method is used to capture the droplet interface. The simulations capture the spontaneous coalescence and jumping of the droplets. The effect of elasticity and shear-thinning on the coalescence and jumping is investigated at capillary-inertial and viscous regimes. The results reveal that the elasticity of the droplet changes the known capillary-inertial velocity scaling of the Newtonian drops at large Ohnesorge numbers; the resulting viscoelastic droplet jumps from the surface at larger Ohnesorge numbers than a Newtonian drop, when elasticity amplifies visible shape oscillations of the merged droplet. The numerical results show that polymer chains are stretched during the coalescence and prior to the departure of two drops, and the resulting elastic stresses at the interface induce the jumping of the liquid out of the surface. This study shows that viscoelasticity, typical of many biological and industrial applications, affects the droplet behaviour on superhydrophobic and self-cleaning surfaces.

1. Introduction

When two droplets coalesce, the total surface area decreases. Hence, surface energy is released during this process. If the two droplets are far from a wall, the new bigger drop oscillates symmetrically until the released surface energy has been dissipated by viscosity. However, when two drops of micro- or nanometer size coalesce on a superhydrophobic surface, the presence of a repellent wall breaks the vertical symmetry and the resulting droplet propels in the direction perpendicular to the wall [1]. Coalescence-induced jumping has been reported on a variety of natural repellent surfaces such as cicada, lacewings [2] and gecko skin [3], and can be exploited in a variety of applications such as anti-icing [4] and self-cleaning surfaces [2,3], and to control heat transfer [5]. Several researchers have studied the different aspects of the coalescence-induced droplet jumping numerically and experimentally, including the basic mechanism of the two equal-sized drop self-propelled jumping [6], and the effects of droplet size mismatch [7,8], droplet initial velocity [9,10], surface topology [11–15], surrounding gas properties [16–18], and surface wettability [19]. A few main results are outlined in the following.

When two equal-sized static drops coalesce on a superhydrophobic surface, their total surface area decreases. This implies that surface energy is released and converted into viscous dissipation and kinetic energy, in a proportion determined by the Ohnesorge number, which represents the ratio between viscous and capillary-inertial forces. At large Ohnesorge numbers, corresponding to the viscous regime, the kinetic energy is completely absorbed by viscous forces, preventing the jumping of the merged droplet [6]. Even at small Ohnesorge numbers, corresponding to the capillary-inertial regime, only less than 4% of the released surface energy converts to vertical translational kinetic energy, which nevertheless causes the jumping of the merged droplet. The conversion rate of surface energy into kinetic energy reduces when the droplets are of unequal sizes, due to the strong asymmetric flow [7,8]. The merged droplet attains an asymmetric shape and jumps with an oblique angle when one of the two droplets has an initial velocity; moreover, the jumping velocity of the merged droplet increases significantly above a critical initial velocity [10].

In addition, macrostructures on the surface affect the jumping velocity and energy transfer rates significantly. The jumping velocity and the conversion efficiency of surface energy to kinetic energy decrease if the lower contour of the merging drop falls between the gap of two rectangular grooves, whereas both jumping velocity and energy conversion increase when the liquid bridge expands on a triangular

---

* Corresponding author.
E-mail address: kazemba@mech.kth.se (K. Bazesefidpar).

prism structure [11]. The critical Ohnesorge number for droplet jumping depends on both the surface wettability and the ambient fluid properties such as density and viscosity; in particular, a larger density contrast between the ambient and drops will cause the merged droplet to jump higher [16].

A moving contact line forms when the interface of two immiscible fluids intersects a solid wall, and the elasticity of the drop speeds up the contact line motion [20–22]. The viscoelastic drops coalesce faster than the Newtonian drops, and the elasticity of the drops expedite the film drainage [23,24]. In very recent experiments, the effect of the drops' elasticity on the coalescence process was studied for both freely suspended drops and sessile drops with radius $O(1)$ micrometer on the hydrophobic surfaces [25]. They found that elasticity enhances the curvature of connecting bridge between two merging drops, and polymer stresses remain confined in a small region around the liquid bridge between the coalescing drops. However, the induced elastic stresses were found to be insufficient to alter the temporal evolution of the bridge in the capillary-inertial regime, and hence elasticity did not change the flow regime.

In the present work, we perform numerical simulations to study the effects of the non-Newtonian viscoelastic properties of two equal-sized static droplets on the coalescence-induced droplet jumping at large Ohnesorge numbers. Our studies extend from the viscous–capillary to the inertial-capillary regime, and in the former case we do observe prominent changes due to elasticity. We use the Cahn–Hilliard Phase-Field method for capturing the interface between the two phases, and the Giesekus constitutive equation to model both the viscoelasticity and shear-thinning of the drops. First, the role of elasticity is investigated by comparing the vertical velocity and different components of energy for a Newtonian and Oldroyd-B droplet at the same Ohnesorge number based on the same zero shear viscosity, while the influence of the liquid shear-thinning rheology is examined by using Giesekus model.

2. Governing equations and numerical methods

The numerical method used in this work has been described in detail in Bazesefidpar et al. [26], so we only give a brief outline here. We consider two immiscible fluids with different densities and viscosities. The outer fluid is Newtonian with viscosity μ_n, whereas the droplets consist of a Giesekus fluid with solvent viscosity μ_s, polymeric viscosity μ_p, and the other non-Newtonian rheological properties as below. To distinguish between the phases, we introduce a phase-field variable, where $\phi = \pm 1$ in the bulk fluids and $\phi = 0$ at the fluid/fluid interface. This problem can be modelled with the following coupled equations [27,28]:

$$\rho\left(\frac{\partial \mathbf{u}}{\partial t} + (\mathbf{u} \cdot \nabla)\mathbf{u}\right) + \mathbf{J} \cdot \nabla \mathbf{u} = -\nabla p + \nabla \cdot \boldsymbol{\tau} + \nabla \cdot \mu_s(\nabla \mathbf{u} + \nabla \mathbf{u}^T) + G\nabla\phi, \quad (1)$$

$$\nabla \cdot \mathbf{u} = 0, \quad (2)$$

the Cahn–Hilliard model:

$$\frac{\partial \phi}{\partial t} + \nabla \cdot (\mathbf{u}\phi) = \nabla \cdot (M\nabla G), \quad (3)$$

$$G = \lambda\left(-\nabla^2\phi + \frac{1}{\eta^2}\phi(\phi^2 - 1)\right), \quad (4)$$

and the Giesekus constitutive model:

$$\boldsymbol{\tau}_p + \lambda_H\left(\frac{\partial \boldsymbol{\tau}_p}{\partial t} + \mathbf{u} \cdot \nabla \boldsymbol{\tau_p} - \boldsymbol{\tau}_p\nabla\mathbf{u} - \nabla\mathbf{u}^T\boldsymbol{\tau}_p\right) + \frac{\alpha\lambda_H}{\mu_p}(\boldsymbol{\tau}_p \cdot \boldsymbol{\tau}_p) =$$

$$\mu_p(\nabla\mathbf{u} + \nabla\mathbf{u}^T), \quad (5)$$

$$\boldsymbol{\tau} = \frac{(1+\phi)}{2}\boldsymbol{\tau}_p, \quad (6)$$

In the above equations, $\mathbf{u}(\mathbf{x}, t)$ is the velocity vector, $p(\mathbf{x}, t)$ is the pressure, and $\boldsymbol{\tau}(\mathbf{x}, t)$ is the extra stress due to the polymers, equal to
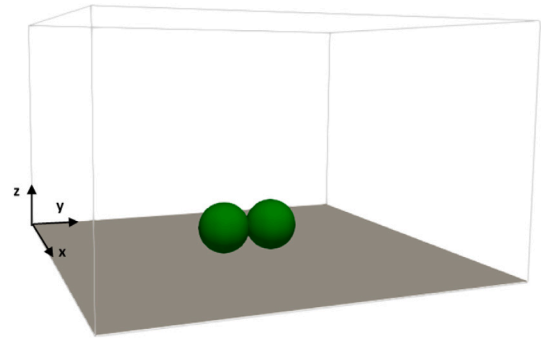

Fig. 1. Sketch of the chosen computational domain Ω_1.

$\boldsymbol{\tau}_p$ inside the droplet and 0 outside (see Eq. (6)). In the Cahn–Hilliard equation, G is the chemical potential, M is the mobility parameter, and η is the capillary width of the interface. In the Giesekus model, $\boldsymbol{\tau}_p$ is the polymer stress, λ_H is the polymer relaxation time, α is the Giesekus mobility parameter, and the polymeric retardation time can be related to the polymeric relaxation time by $\lambda_r = \frac{\mu_s}{\mu_s+\mu_p}\lambda_H$. In Eq. (4), λ is the mixing energy density, and it is related to the surface tension in the sharp-interface limit [27] by:

$$\sigma = \frac{2\sqrt{2}}{3}\frac{\lambda}{\eta} \quad (7)$$

Fluid 1 indicates the droplet phase and fluid 2 represents the surrounding fluid (air). The density ρ and the dynamic viscosity μ fields are expressed using the phase-field variable as:

$$\rho = \frac{(1+\phi)}{2}\rho_1 + \frac{(1-\phi)}{2}\rho_2, \quad (8)$$

$$\mu = \frac{(1+\phi)}{2}\mu_{s_1} + \frac{(1-\phi)}{2}\mu_{s_2}, \quad (9)$$

The total viscosity of the non-Newtonian phase is $\mu_t = \mu_s + \mu_p$. The density satisfies the following relation [28]

$$\frac{\partial \rho}{\partial t} + \nabla \cdot \rho\mathbf{u} = -\nabla \cdot \mathbf{J}, \quad (10)$$

where $\mathbf{J} = -\frac{(\rho_1-\rho_2)}{2}M\nabla G$. Boundary conditions imposed on the substrate are, following Jacqmin [29] and Qian et al. [30], the no-slip boundary condition for the velocities:

$$\boldsymbol{u} = \mathbf{0}, \quad (11)$$

and the static contact angle θ_s for the phase-field variable:

$$\mathbf{n} \cdot \nabla\phi + \frac{1}{\lambda}f'_w(\phi) = 0, \quad (12)$$

$$f_w(\phi) = \sigma\cos(\theta_s)\frac{\phi(\phi^2 - 3)}{4} + \frac{(\sigma_{w_1} + \sigma_{w_2})}{2}, \quad (13)$$

where $\mathbf{n}$ is the outward pointing normal vector to the boundary, and $f_w(\phi)$ is a function describing the fluid–solid interfacial tension.

A second-order accurate scheme is employed for the temporal discretization of Eq. (3) and (1) while a semi-implicit splitting scheme is used to treat the linear parts implicitly and the non-linear parts explicitly [31]. To avoid the High-Weissenberg number problem (HWNP), the log-conformation reformulation (LCR) of equation Eq. (5) [32,33] is used and advanced in time by a second-order total variation diminishing (TVD) Runge–Kutta method [34]. Finally, we use second-order central differences to approximate spatial derivatives, except for the advection terms in Eqs. (3) and (5), where the fifth-order WENO-Z is used to improve stability and accuracy [35].
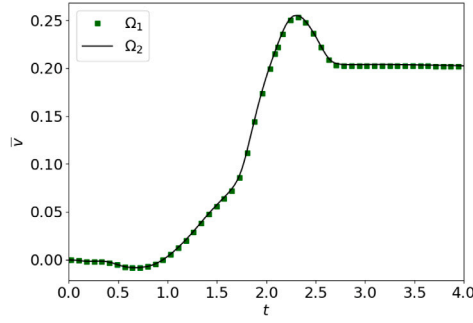
Fig. 2. Average velocity integrated over the droplet volume in time, for the chosen domain (stars) and a bigger domain Ω_2 (solid line), to show independence of the domain size. The parameters are $Oh = 0.0076$ and $De = 10$.
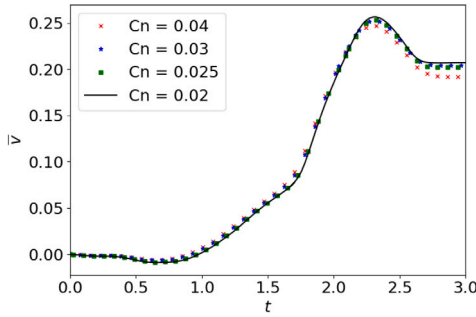

Fig. 3. The evaluation of average velocity of the merged viscoelastic droplet for different Cn numbers.

3. Physical model and computational domain

We consider two equal-sized initially static viscoelastic drops touching a homogeneous surface (Fig. 1) with a static contact angle of $180°$, and we ignore the adhesion between the droplets and the wall. When two adjacent droplets coalesce on a superhydrophobic surface, the formed liquid bridge impinges on the substrate, and the merged droplet may jump above the substrate. Here, gravity is neglected, because the droplet radius is assumed to be much smaller than the capillary length and therefore capillary forces are expected to dominate.

The capillary-inertial velocity is chosen as the velocity scale [1] $u_{ci} = \sqrt{\sigma / (\rho_1 r_0)}$, the droplets initial radius r_0 as the length scale, the inertial-capillary time $\tau_{ci} = \sqrt{(\rho_1 r_0^3)/\sigma}$ as the time scale, the droplet density ρ_1 as the reference density, and the droplet viscosity μ_1 as the reference viscosity. This gives rise to seven nondimensional numbers. Firstly, the Ohnesorge number $Oh = \left(\mu_1/\sqrt{\rho_1 \sigma r_0}\right)$ representing the relative importance of viscous to capillary-inertial forces; the Weissenberg number $Wi = \left(\lambda_H u_{ci}/r_0\right)$ representing the ratio between elastic and viscous forces; the Peclet number $Pe = \left(2\sqrt{2} u_{ci} r_0 \eta\right)/(3M\sigma)$ representing the ratio between the advection and diffusion in the Cahn–Hilliard equation. Furthermore, the Cahn number $Cn = (\eta/r_0)$ is the ratio between the interface width and the characteristic length scale; $\beta = \mu_s/\left(\mu_s + \mu_p\right)$ is the ratio between the solvent viscosity and total viscosity; $k_\mu = (\mu_2/\mu_1)$ is the ratio between the ambient and droplet viscosities; $k_\rho = (\rho_2/\rho_1)$ between the ambient and droplet densities. The different components of the energy are scaled by σr_0^2. In what follows, all quantities will be nondimensional unless indicated otherwise.

To quantify the role of the fluid elasticity on the droplet jumping, we will measure the mass-averaged velocity of the droplet, defined as:

$$\bar{v} = \frac{\int_\Omega \frac{1}{2}(1+\phi) v_z \, d\Omega}{\int_\Omega \frac{1}{2}(1+\phi) d\Omega} \tag{14}$$

r_0 (µm)	ρ_1 $\left(\frac{\text{kg}}{\text{m}^3}\right)$	μ_1 (Pa s)	σ $\left(\frac{\text{N}}{\text{m}}\right)$	k_ρ	k_μ	θ_a^{app}	θ_r^{app}	$\Delta\theta^{app}$
290	998.2	0.001	0.072	$\frac{1}{839}$	$\frac{1}{58.8}$	170.3°	167.7°	2.6°

where Ω is the computational domain (see Fig. 1), and z the direction perpendicular to the solid substrate. We also analyse the different components of the energy during the coalescence and jumping. The total energy E_T of an Oldroyd-B fluid excluding the solid–fluid surface energy is the sum of the surface energy E_s, kinetic energy E_k, and elastic energy E_e, defined in phase-field framework as [36,37]:

$$E_s = \int_\Omega \frac{3Cn}{4\sqrt{2}}\left[|\nabla\phi|^2 + \frac{1}{2Cn^2}(\phi^2 - 1)^2\right] d\Omega,$$

$$E_k = \int_\Omega \frac{1}{4}(1+\phi)\mathbf{u}\cdot\mathbf{u} \, d\Omega, \tag{15}$$

$$E_e = \int_\Omega \frac{Oh}{2}\frac{(1-\beta)}{Wi}\text{tr}(\mathbf{c} - \ln\mathbf{c} - \mathbf{I}) \, d\Omega,$$

$$E_T = E_s + E_k + E_e,$$

where the relationship between polymer stress $\boldsymbol{\tau_p}$ and the conformation tensor $\mathbf{c}$ is

$$\boldsymbol{\tau_p} = \frac{(1-\beta)}{Wi}(\mathbf{c} - \mathbf{I}), \tag{16}$$

The part of the kinetic energy associated to the vertical velocity component is most relevant here as it can be associated with the jumping motion, while the rest is related to interface oscillatory motions [6]. We will therefore consider a translational kinetic energy, defined as,

$$E_{k,tr} = \int_\Omega \frac{1}{2}(1+\phi)\bar{v}^2 \, d\Omega \tag{17}$$

where $\bar{v}$ is the droplet mass-averaged velocity in z-direction, and $E_{k,os} = E_k - E_{k,tr}$ is the part of the kinetic energy associated with the oscillatory motion.

The numerical setup is as follows. The nondimensional domain size is chosen of size $\Omega = [0, 10] \times [0, 10] \times [0, 8]$. Two adjacent droplets with initial radius 1 are placed above the x–y plane at z = 0, see Fig. 1. We impose no-slip and no-penetration conditions on the two boundaries in the z-direction, with static contact angles $\theta_s = 180°$ at the bottom wall and $\frac{\partial\phi}{\partial n} = 0$ at the top boundary.

Periodic boundary conditions are applied for all variables in the x- and y-directions. We use 8 grid points across the nominal interface in order to resolve the sharp gradients, and set the Peclet number to $Pe = \frac{6}{Cn}$, according to the guidelines in Magaletti et al. [38], Xu et al. [39] and Yue et al. [40] to approach the sharp-interface limit.

To ensure that the chosen grid and domain size are sufficient, we performed the following numerical tests. Firstly, we examined the effect of the computational domain on the velocity of the merged droplet by performing an additional simulation on a larger domain $\Omega_2 = [0, 15] \times [0, 15] \times [0, 9]$; the results obtained on Ω_1 match those obtained on the larger domain Ω_2, as shown in Fig. 2. We also tested the grid dependency of the results by comparing the averaged velocity of the merged viscoelastic droplet for four different resolutions corresponding to different values of the Cahn number. For this test, the following values of the dimensionless numbers introduced above were used:

$$Oh = 0.0076, \quad Wi = 10, \quad \beta = 0.1, \quad k_\mu = 0.017, \quad k_\rho = 0.00119.$$

Fig. 3 shows that the averaged velocity of the merged drop with $Cn = 0.025$ is almost the same as that obtained with the finer grid $Cn = 0.02$. Higher values of Cn displays non-negligible differences when the simulation time exceeds 2. Thus, we choose $Cn = 0.025$, corresponding to a grid with $N_x \times N_y \times N_z = 760 \times 760 \times 608$ grid points. This satisfactory convergence is achieved adopting the scaling between the Peclet number and Cn number suggested by [38,39].
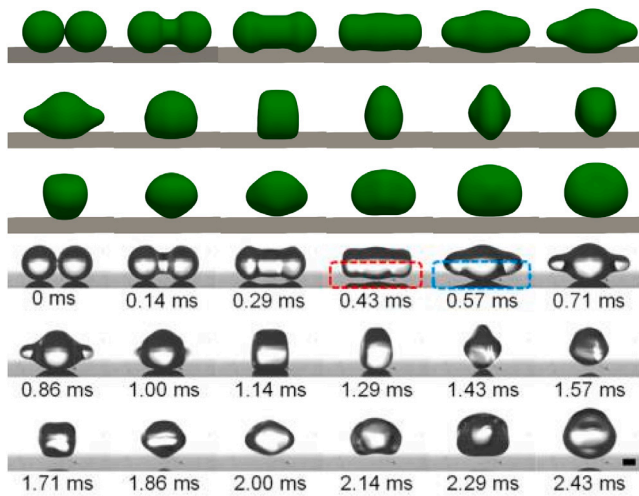
Fig. 4. The coalescence and jumping of two Newtonian droplets on a superhydrophobic surface at $Oh = 0.0076$: (a) Numerical results from present work (yz view) (b) Experimental data of Yan et al. [18].

4. Results

For the results presented here, the density ratio and viscosity ratio are kept constant ro $k_\rho = \frac{1}{839}$ and $k_\mu = \frac{1}{58.8}$., following the values from the experiments in Yan et al. [18].

4.1. Newtonian droplets — comparison with experiments

The solver has been validated against several Newtonian and viscoelastic two-phase flow benchmarks in 2D and 3D [26]. Here, we compare the spontaneous coalescence and jumping motion of a Newtonian drop on a superhydrophobic surface with the experimental data of Yan et al. [18]. We choose the same physical parameters as in the experiment, see Table 1. The influence of the solid–liquid adhesion on the self-propelled jumping is negligible when the contact angle hysteresis ($\Delta\theta^{app}$) is less than 10° [17,41], so we ignore the contact angle hysteresis and impose a static contact angle $\theta_s = 180°$ on the bottom wall. Fig. 4 presents the experimental data [18] for the coalescence of two Newtonian drops on a superhydrophobic surface and the corresponding numerical results; the visualization shows that the numerical simulation is able to capture the coalescence and jumping process accurately in time.

The jumping velocity of the merged water (Newtonian) drop on a superhydrophobic surface is constant in the capillary-inertial region (i.e., $Oh \lesssim 0.1$); [1] reported $v_j \approx 0.2$ for the water drop at 19 °C on a textured superhydrophobic surface. Later, [18] reduced the level of undesired external disturbances and measured a velocity $v_j \approx 0.26$ for self-propelled jumping of water drops upon coalescence on a superhydrophobic surface. Fig. 5(a) shows the averaged velocity of the merged droplet in our simulation. The jumping velocity is measured from the time the bottom of the merged drop leaves the surface. Liu et al. [6] suggested that a sensible time for extracting the jumping velocity is the first pseudo-equilibrium, which corresponds to the time when the axial lengths of the merged droplet in x- and y-directions become equal. These axial lengths are measured with respect to an axis attached to the centre of mass of the merged drop, and density ratio in their numerical simulation was $k_\rho = 0.02$. Following this criterion, the jumping velocity of the Newtonian drop at $Oh = 0.0076$ is $v_j \approx 0.21$ in our simulations. It should be noted that the criterion of Liu et al. [6] may work less well at our high density ratios, since the merged droplet's average velocity decreases very rapidly after its maximum, and this may lead us to underestimate the jumping velocity.

The dimensionless time corresponding to the first pseudo-equilibrium is $t \approx 3.32$ (dimensional time $t^* \approx 1.92$ ms) with the droplet leaving the surface at $t \approx 2.71$ ($t^* \approx 1.57$ ms) in both simulation and experiment. The averaged velocity at $t = 2.71$ is $\bar{v} \approx 0.23$, and the maximum averaged velocity is $\bar{v}_{max} \approx 0.26$, see Fig. 5(a).

Fig. 5(b) presents the time-evolution of the total and surface energy of the merging and jumping droplet. The total energy of the droplet decreases over time due to the viscous dissipation, and this decrease is larger in the merging process and prior to jumping, because there are highly localized velocity gradients around the liquid bridge during its impingement on the substrate. Fig. 5(c) depicts the total and translational kinetic energy of the merged droplet, confirming that a small fraction of the released surface energy is converted into transitional kinetic associated to the jumping motion.

4.2. Viscoelastic droplets — elasticity effect

Most of the existing studies are restricted to experiments with water droplets and numerical simulation of Newtonian drops; [18] newly investigated the effect of the liquid internal hydrodynamics by conducting experiment for the self-propelled jumping upon coalescence on a superhydrophobic surface with ethanol–water and ethylene-glycol solutions. Their experiment shows that the properties of the droplet affect the coalescence and jumping process significantly. A very recent experimental study, however, addressed the effect of the drops' elasticity on the coalescence process [25], and their findings will be referred to later in this section. In the following, we investigate numerically how the droplet elasticity (Weissenberg number) influences the jumping process for different values of the Ohnesorge number. One way to vary the Ohnesorge number in experiments is to keep the physical properties constant and vary the droplet radius, and we adopt this approach in our simulation for the Newtonian drops. However, we change the polymeric relaxation time λ_H in the simulation in addition to droplet radius for the viscoelastic droplets in order to keep the Weissenberg number constant, since it depends on the droplet radius. It should be noted that other parameters change with the droplet radius; the parameters for each case are summarized in Appendix.

4.2.1. Small ohnesorge numbers

To isolate the effect of the droplet elasticity on the coalescence and jumping on a superhydrophobic surface in the inertial-capillary region, $Oh \lesssim 0.1$, we set $\alpha = 0$ in the following simulations. This choice implies that shear-thinning is eliminated, and the Giesekus model reduces to the Oldroyd-B model. The average velocities of the merged Newtonian and viscoelastic droplets are compared at two Ohnesorge numbers, $Oh = 0.0076$ and $Oh = 0.0373$. For Newtonian droplets, these values represent the capillary-inertial regime. The two dimensionless numbers defining the Oldroyd-B model are kept constant, $Wi = 10$ and $\beta = 0.1$, see Appendix.

Fig. 6(a) shows the time evolution of the average velocity of the merged droplet for the Newtonian and viscoelastic cases, for both Ohnesorge numbers. The first observation is that both droplets jump from the surface at these low Ohnesorge numbers. Let us now consider the blue lines, corresponding to the smallest Ohnesorge number: Newtonian (solid line) and viscoelastic (dashed line). We observe that the elasticity of the drop has a negligible effect on the average velocity prior to and during jumping. However, there is a small qualitative difference after jumping, where the averaged velocity remains approximately constant for the viscoelastic droplet, while the velocity of the Newtonian droplet decreases in time. For the larger Ohnesorge number (green lines), we observe that the droplet elasticity increases the maximum averaged velocity. The total energy is dissipated more rapidly in the Newtonian droplet after departure, while there is less dissipation in the merged viscoelastic droplet, see Fig. 6(b). The droplet kinetic energy is presented in Fig. 6(c): the viscoelastic droplet has more kinetic energy so that it undergoes larger shape oscillations than the Newtonian droplet.
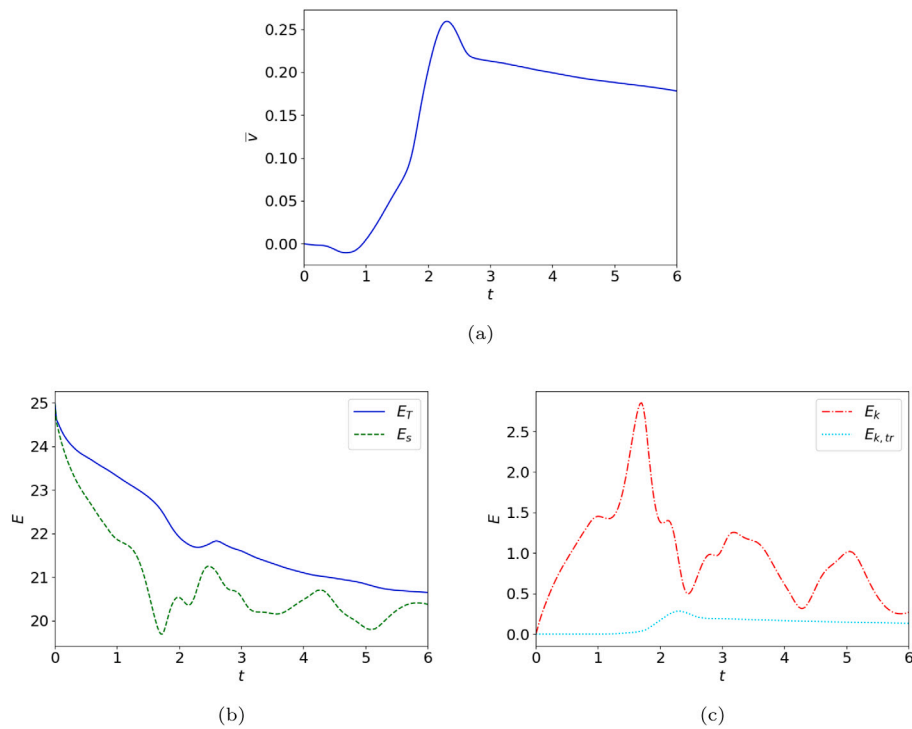
Fig. 5. Time-dependent quantities of the Newtonian merged drop on a superhydrophobic surface at $Oh = 0.0076$: (a) The average velocity, (b) Total and surface energies of the merged drop (c) Kinetic and translational kinetic energies of the merged drop.
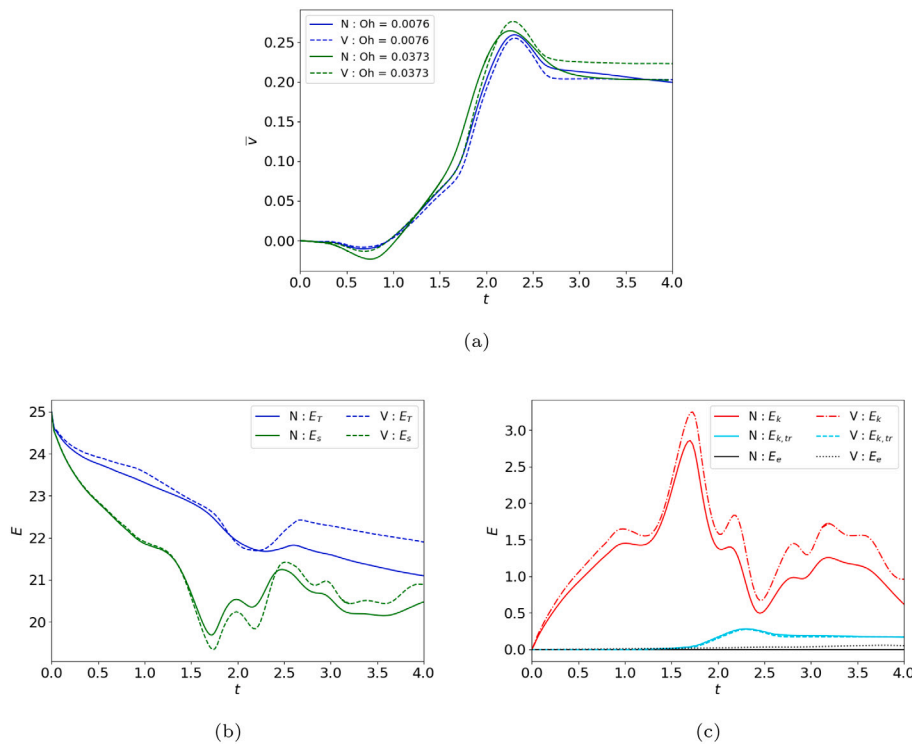

Fig. 6. Quantities of the merged Newtonian and Oldroyd-B drops at $Wi = 10$ and $\beta = 0.1$. N and V refer to Newtonian and Oldroyd-B drops respectively. (a) The averaged velocity (b) Total and surface energies of the merged drop at $Oh = 0.0076$ (c) Kinetic and transitional kinetic energies of the merged drop at $Oh = 0.0076$.

The oscillations of the viscoelastic droplet are due to its elasticity and independent of the surface tension, see [42]. The viscoelastic droplet oscillates even at the large Ohnesorge numbers corresponding to a highly viscous drop [42]. An extensional flow occurs when the two viscoelastic drops are coalescing, so polymer chains stretch and store elastic energy during the coalescence process, see Fig. 6(c).

Summarizing, the average and jumping velocity are not considerably affected by the elasticity of the drops in the inertial-capillary regime. This result is in line with the experiments of Dekker et al. [25], where elasticity did not considerably influence the coalescence process in the inertial-capillary regime. However, quantitatively we found that the oscillations are promoted by elasticity, and that the
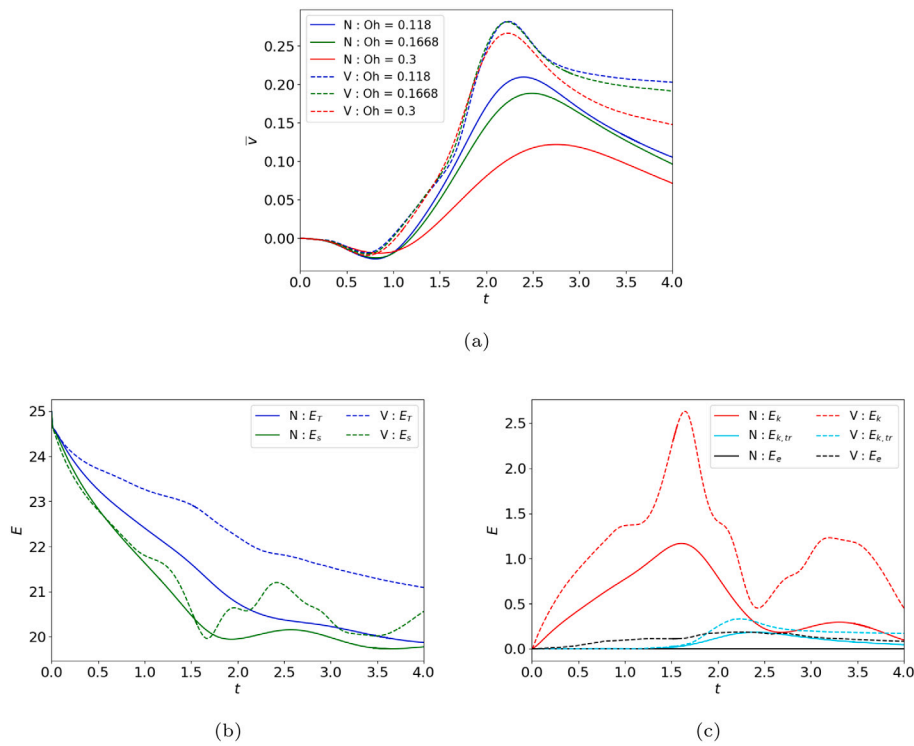
Fig. 7. Quantities of the merged Newtonian and Oldroyd-B drops at $Wi = 10$ and $\beta = 0.1$. N and V refer to Newtonian and Oldroyd-B drops respectively. (a) The averaged velocity (b) Total and surface energies of the merged drop at $Oh = 0.118$ (c) Kinetic and transitional kinetic energies of the merged drop at $Oh = 0.118$.
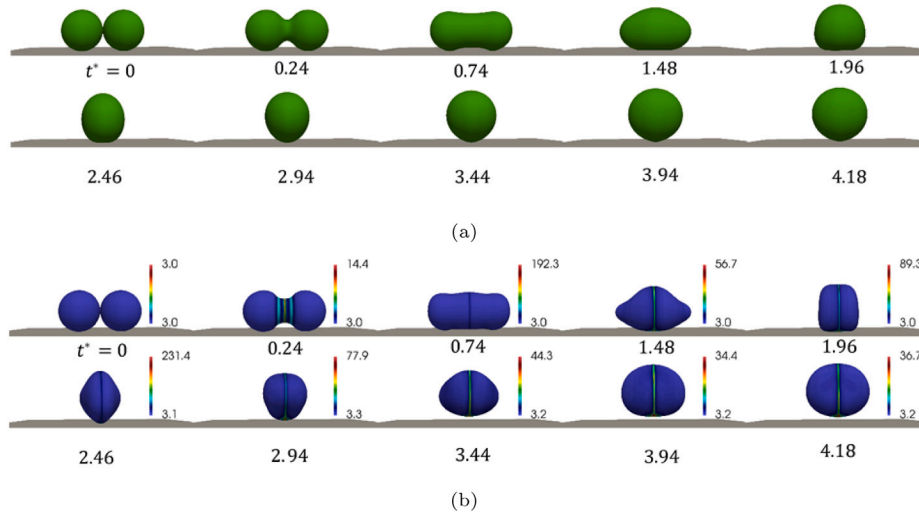

Fig. 8. The coalescence and jumping of Newtonian and Oldroyd-B drops on a superhydrophobic surface at $Oh = 0.118$, $Wi = 10$ and $\beta = 0.1$ (a) Newtonian drops (b) Oldroyd-B drops. The trace of the dimensionless polymeric stresses are visualized on the surface of the polymeric drop.

average velocity decays less rapidly after the droplet departure from the superhydrophobic surface.

4.2.2. Large ohnesorge numbers

For Newtonian drops, viscous forces become the dominant at larger Ohnesorge numbers ($Oh \gtrsim 0.1$), known as the viscous regime: both jumping and averaged velocities decrease rapidly with increasing Ohnesorge number due to the strong viscous dissipation. Let us now examine whether and how this behaviour changes for viscoelastic droplets at $Oh \gtrsim 0.1$.

The results from the simulations are reported in Fig. 7. First, we note that the merged viscoelastic droplet gains much larger average velocity than the Newtonian one during the coalescence process, as

seen by comparing the solid (Newtonian) and dashed (viscoelastic) lines of the same colour in panel (a). Panel (b) of the same figure shows that the released energy is soon damped at $Oh = 0.118$ ($t^* \approx 4$), and the total energy (blue solid line) reaches its equilibrium value $E_T^* = 2^{\frac{2}{3}} 4\pi$ consisting of surface energy only (green solid line). The Newtonian drop resulting from the coalescence reaches a spherical shape corresponding to its equilibrium, and stays on the surface without jumping, as shown in Fig. 8.

Let us now consider the polymeric drop (dashed blue and green lines). This merged polymeric drop has energy available to oscillate and move upwards. The kinetic energies of the Newtonian (solid) and Oldroyd-B droplets (dashed) are depicted in Fig. 7(c), and both total and translational kinetic energies of the polymeric drop are

larger than for the Newtonian drop. The Oldroyd-B drop also has the additional elastic energy due to the presence of the polymer molecules, see the black dashed line. These are stretched during the coalescence and prior to jumping, so that extra elastic energy is stored and available for the polymeric drop.

A visualization of the coalescence and jumping of both droplets at $Oh = 0.118$ is provided in Fig. 8. The polymeric drops merge faster than the Newtonian drops, and the bridge formed due to the coalescence reaches the substrate sooner. The interface (given by $\phi = 0$) of the Oldroyd-B drops is coloured using the trace of the conformation tensor which indicates the intensity of polymer stretching. As reported in experiments of [25], the polymeric stresses are seen to be very concentrated around the merging interface and the capillary bridge. At the present flow regime, however, we observe significant changes due to elasticity in both the liquid bridge formation and in the merging and coalescence processes. The merged polymeric drop undergoes a large deformation in all three directions and jumps out of the surface; this oscillatory motion and jumping is characteristic of the inertial-capillary region and is maintained at high Oh when elasticity is present. Indeed, the Newtonian drop goes rapidly towards its equilibrium condition without noticeable oscillations, and remains on the surface, as expected in the viscous region.

To gain a better understanding on the effect of elasticity on the self-propelled jumping, the flow field is visualized on the central XZ and YZ planes inside the merging drops, see Fig. 9(a). As concern the YZ plane, shown in the top row, we depict the interface, identified by the $\phi = 0$ value of the order parameter (red contour), velocity field (arrows), and trace of conformation tensor (colourmap) for merging viscoelastic drop at three times, together with the interface of merging Newtonian drop (white contour). This illustrates how the shape of Newtonian and viscoelastic droplets differ, and confirms the localization of polymeric stresses at the merging cross-section. Moreover, the bottom row of the same figure displays contours of the trace of the conformation tensor for the viscoelastic drops on the XZ plane at the same dimensionless times as in Fig. 9(b). The data indicate that polymers are most elongated prior to jumping, near the bottom wall.

A possible physical explanation for the polymer effect can be as follows. When the two initially static drops start to merge, the liquid moves driven by the capillary pressure towards the centre of the expanding bridge. Then, due to the conservation of mass, the liquid is forced to move in the transverse XZ plane, see the velocity field of the merging viscoelastic drops in Fig. 9(b) at $t = 0.24$. This flow causes the polymer molecules to stretch in the XZ plane and produce extra elastic stresses, which push the liquid bridge connecting the two polymeric drops to move faster. When the liquid bridge interacts with the substrate at $t \approx 1$, the liquid is induced to move upwards due to the impermeability of the surface. This upward flow converges towards the XZ plane and causes the polymers to stretch mainly in the vicinity of the substrate, as shown by the trace of conformation tensor at $t = 1.96$ in Fig. 9(b). The stretched polymers exert extra elastic stresses on the interface near the substrate, so the merged polymeric drop jumps out of the surface. The newly-formed larger drop leaves the surface at $t \gtrsim 3$, when the trace of the conformation tensor decreases. Later, the polymers are mainly stretched at the bottom of the merged drop, and two small vortices appear in that region so that the polymer molecules remain stretched. Thus, these extra polymer stresses at the bottom of the drop push the drop to move upward. The polymers are also significantly stretched in the XZ plane around the interface, and these extra polymer stresses push the interface to oscillate in the x-direction, see Fig. 9(b).

These results reveal that the elasticity of the drop plays an important role at large Ohnesorge numbers in the coalescence and jumping process of two initially static equal-sized polymer drops on a superhydrophobic surface; elasticity also affects the merged droplet motion after its departure as demonstrated by the oscillatory motion in highly-viscous yet viscoelastic drops.

4.3. Viscoelastic droplets — effects of polymeric viscosity ratio and shear-thinning

The effect of the shear thinning on the self-propelled jumping of two equal-sized polymeric drops has been studied by performing simulations at $Oh = 0.118$, $De = 10$, $\beta = 0.1$ and varying α; the results show that the effect of shear thinning is minor and negligible for the self-propelled jumping of two equal-sized polymeric drops even at large Ohnesorge numbers, see Fig. 10. This can be explained by the fact that the velocity gradients are mainly localized around the liquid bridge so that the effect of shear-thinning is negligible.

In addition, we have investigated the effect of the polymeric viscosity ratio β on the self-propelled jumping at $Oh = 0.118$ and $Wi = 10$. Fig. 11 depicts the variation of the averaged velocity of the droplet for $\beta = 0.1 - 0.8$. The Newtonian droplet velocity is also shown for comparison. Two regimes can be distinguished: as long as $\beta \lesssim 0.5$, we note a minor influence on the averaged velocity; for $\beta \gtrsim 0.6$, conversely, the velocity rapidly converges towards the Newtonian one, so that elasticity effects become negligible. This can be explained by considering the retardation time, *i.e.* the relative time it takes for polymer molecules to be stretched. The retardation time can be related to the polymeric viscosity ratio by $\lambda_r = \beta \lambda_H$, while the flow time scale time is constant in our simulations since the droplet radius r_0, velocity scale $u_{ref} = \sqrt{\frac{\sigma}{\rho_1 r_0}}$, and Weissenberg number Wi are kept constant. Since the retardation time is increasing by increasing β, the polymers do not have time to stretch and store elastic energy during the coalescence and jumping when $\beta \gtrsim 0.6$. Thus, the polymeric drops behave like Newtonian drops at large polymeric viscosity ratios.

Finally, the average velocities of two merged Newtonian drops at two Ohnesorge numbers, $Oh = 0.1668$ and $Oh = 0.01668$, and an Oldroyd-B drop with dimensionless numbers, $Oh = 0.1668$ and $Wi = 10$ are compared to investigate the effect of polymers on top of the solvent, see Fig. 12. In the case of $Oh = 0.01668$, all the parameters are the same as the Newtonian case with $Oh = 0.1668$ except that the viscosity of the droplets has been chosen to be ten times smaller, the same as solvent viscosity of viscoelastic drops. The average velocity of merging Newtonian droplets at $Oh = 0.01668$ and viscoelastic droplets at $Oh = 0.1668$ are approximately the same for $t \lesssim 1.5$ since the polymer stresses are still building up and are not yet able to store visible amounts of elastic energy. Two curves deviate from each other for $t \gtrsim 1.5$, and the average velocity of the merging viscoelastic drops increases due to the presence of stretched polymer molecules. As expected, the average velocity of merging Newtonian drops at $Oh = 0.1668$ decays very rapidly due to viscous dissipation.

5. Conclusions and outlook

In the present study, three-dimensional direct numerical simulations have been performed to study the self-propelled jumping of two equal-sized polymeric drops on a superhydrophobic surface with contact angle of 180°. The results demonstrate that the viscoelastic properties of the droplets have a significant impact on the coalescence and jumping.

At small Ohnesorge numbers (inertial-capillary region), the elasticity effect is weak before the jumping; however, the averaged velocity of the coalesced drop does not decay as rapidly as for a Newtonian liquid. Drop shape oscillations are promoted by the presence of the polymers.

At large Ohnesorge numbers ($Oh \gtrsim 0.1$) however, profound differences between polymeric and Newtonian drops are observed during the coalescence and jumping process. The polymeric drops merge faster than the Newtonian drops, and the merged drop jumps out of the surface in contrast to their Newtonian counterparts, which remains on the substrate due to the large viscous dissipation. Our investigation reveals that the polymers are highly stretched at the cross-section of the merging droplets during coalescence, and these stretched chains exert extra elastic stresses on the interface of the merging drops in the vicinity of the wall, hence helping the polymeric drop to jump from the
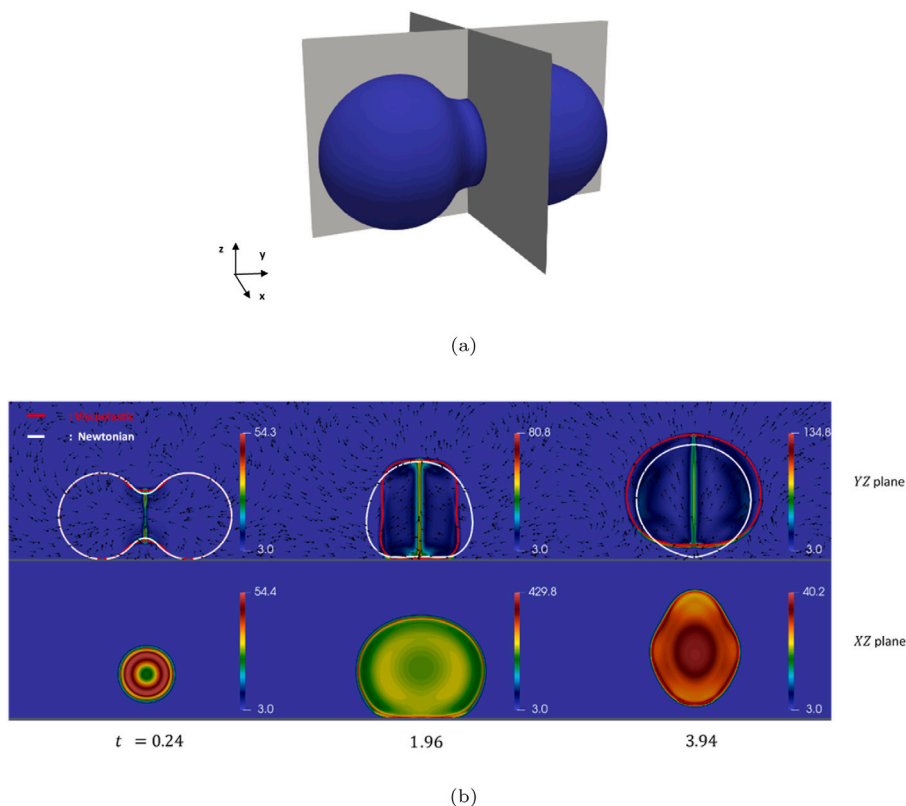
(a)

(b)

Fig. 9. Time evolution of viscoelastic drops coalescence on XZ and YZ planes on a superhydrophobic surface at $Oh = 0.118$, $Wi = 10$ and $\beta = 0.1$. The interface $\phi = 0$ of the merging Newtonian drops are depicted at $Oh = 0.118$ on YZ plane for the comparison : (a) XZ and YZ planes used for the visualization of the flow field (b) The interface of both Newtonian and viscoelastic drops on YZ plane at three different times t along with the velocity field and trace of conformation tensor belong to the viscoelastic drops. The trace of conformation tensor is visualized on XZ for the viscoelastic drops.
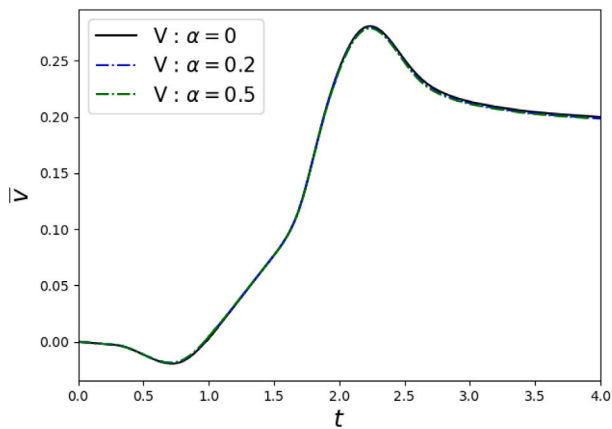

Fig. 10. The effect of drop shear-thinning α on the averaged velocity at $Oh = 0.118$, $Wi = 10$, and $\beta = 0.1$.
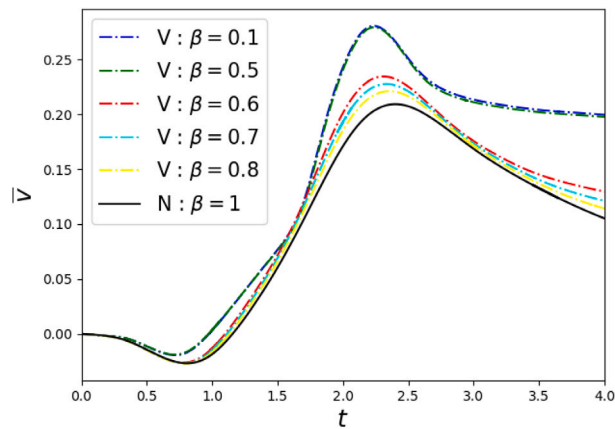

Fig. 11. The effect of polymeric viscosity ratio β on the averaged velocity at $Oh = 0.118$ and $Wi = 10$.

surface. These results are obtained with a typical value in the literature for the polymeric viscosity ratio, i.e. $\beta = 0.1$; here, we also observe that the merged viscoelastic drop behaves like a Newtonian drop when $\beta \gtrsim 0.7$. The larger β corresponds to larger retardation times in our simulation, so that the polymer molecules do not have enough time to stretch. Finally, the shear-thinning effect is found to be negligible in the coalescence and jumping process of two equal-sized drops on a superhydrophobic surface.

Our results indicate that the elasticity of the droplet can change the viscous cutoff radius (for example 30 μm for water) for the self-propelled jumping of drops on superhydrophobic surfaces. Thus, it is expected that polymeric drops jump from a superhydrophobic surface upon their coalescence with radii below the viscous cutoff radius for Newtonian drops at the same Ohnesorge number. Moreover, the merged polymeric drop oscillatory motion is promoted by the elasticity of the drop in both inertial-capillary and viscous–capillary regimes.

In this study, we have neglected the contact angle hysteresis, assuming it to be smaller than 10°; however, superhydrophobic surfaces may have large contact angle hysteresis [43–45], which might play an important role in the case of polymeric drops. The effect of the droplet adhesion with wall also has been neglected in our study. Studying the effect of the contact angle hysteresis and adhesion between droplet and superhydrophobic surfaces are of the possible extensions of this work.
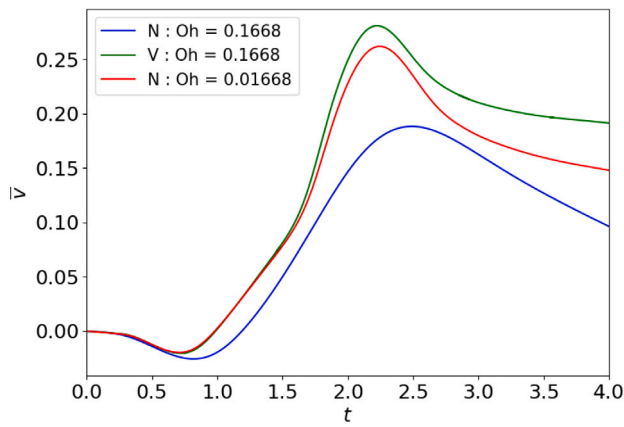
Fig. 12. The effect of polymer on top of the solvent at $Wi = 10$ and $\beta = 0.1$.

Table A.1

Dimensionless numbers used in the simulations at small Ohnesorge numbers, see Section 4.2.1.

Case	Droplets	Oh	Wi	β	α	θ_s^b	k_ρ	k_μ
1	Viscoelastic	0.0076	10	0.1	0	180°	$\frac{1}{839}$	$\frac{1}{58.8}$
2	Newtonian	0.0076	0	1	0	180°	$\frac{1}{839}$	$\frac{1}{58.8}$
3	Viscoelastic	0.0373	10	0.1	0	180°	$\frac{1}{839}$	$\frac{1}{58.8}$
4	Newtonian	0.0373	0	1	0	180°	$\frac{1}{839}$	$\frac{1}{58.8}$

Table A.2

Dimensionless numbers used in the simulations at large Ohnesorge numbers, see Section 4.2.2.

Case	Droplets	Oh	Wi	β	α	θ_s^b	k_ρ	k_μ
1	Viscoelastic	0.118	10	0.1	0	180°	$\frac{1}{839}$	$\frac{1}{58.8}$
2	Newtonian	0.118	0	1	0	180°	$\frac{1}{839}$	$\frac{1}{58.8}$
3	Viscoelastic	0.1668	10	0.1	0	180°	$\frac{1}{839}$	$\frac{1}{58.8}$
4	Newtonian	0.1668	0	1	0	180°	$\frac{1}{839}$	$\frac{1}{58.8}$
5	Viscoelastic	0.3	10	0.1	0	180°	$\frac{1}{839}$	$\frac{1}{58.8}$
6	Newtonian	0.3	0	1	0	180°	$\frac{1}{839}$	$\frac{1}{58.8}$

Table A.3

Dimensionless numbers used in the simulations focusing on the role of shear thinning, see Section 4.3.

Case	Droplets	Oh	Wi	β	α	θ_s^b	k_ρ	k_μ
1	Viscoelastic	0.118	10	0.1	0	180°	$\frac{1}{839}$	$\frac{1}{58.8}$
2	Viscoelastic	0.118	10	0.1	0.2	180°	$\frac{1}{839}$	$\frac{1}{58.8}$
3	Viscoelastic	0.118	10	0.1	0.5	180°	$\frac{1}{839}$	$\frac{1}{58.8}$

Table A.4

Dimensionless numbers used in the simulations focusing on the role of the polymer viscosity ratio, see Section 4.3.

Case	Droplets	Oh	Wi	β	α	θ_s^b	k_ρ	k_μ
1	Newtonian	0.118	0	1	0	180°	$\frac{1}{839}$	$\frac{1}{58.8}$
2	Viscoelastic	0.118	10	0.1	0	180°	$\frac{1}{839}$	$\frac{1}{58.8}$
3	Viscoelastic	0.118	10	0.5	0	180°	$\frac{1}{839}$	$\frac{1}{58.8}$
4	Viscoelastic	0.118	10	0.6	0	180°	$\frac{1}{839}$	$\frac{1}{58.8}$
5	Viscoelastic	0.118	10	0.7	0	180°	$\frac{1}{839}$	$\frac{1}{58.8}$
6	Viscoelastic	0.118	10	0.8	0	180°	$\frac{1}{839}$	$\frac{1}{58.8}$

Table A.5

Dimensionless numbers used in the simulations focusing on the effect of polymer on top of the solvent, see Section 4.3.

Case	Droplets	Oh	Wi	β	α	θ_s^b	k_ρ	k_μ
1	Newtonian	0.1668	0	1	0	180°	$\frac{1}{839}$	$\frac{1}{58.8}$
2	Newtonian	0.01668	0	1	0	180°	$\frac{1}{839}$	$\frac{1}{5.88}$
3	Viscoelastic	0.1668	10	0.1	0	180°	$\frac{1}{839}$	$\frac{1}{58.8}$

Declaration of competing interest

Data availability

Data will be made available on request.

Acknowledgements

Appendix

See Tables A.1–A.5

In this Appendix, we report the values of the non-dimensional numbers used in the simulations.

References

[1] J.B. Boreyko, C.-H. Chen, Self-propelled dropwise condensate on superhydrophobic surfaces, Phys. Rev. Lett. 103 (2) (2009) 184501.

[2] K. Wisdom, J. Watson, X. Qu, F. Liu, G. Watson, C. Chen, Self-cleaning of superhydrophobic surfaces by self-propelled jumping condensate, Proc. Natl. Acad. Sci. 110 (2013) 7992–7997.

[3] G.S. Watson, D.W. Green, L. Schwarzkopf, X. Li, B.W. Cribb, S. Myhra, J.A. Watson, A gecko skin micro/nano structure–a low adhesion, superhydrophobic, anti-wetting, self-cleaning, biocompatible, antibacterial surface, Acta Biomater. 21 (2015) 109–122.

[4] Q. Zhang, M. He, J. Chen, J. Wang, Y. Song, L. Jiang, Anti-icing surfaces based on enhanced self-propelled jumping of condensed water microdroplets, ChemComm 49 (2013) 4516–4518.

[5] R. Enright, N. Miljkovic, J. Alvarado, K. Kim, J. Rose, Dropwise condensation on micro-and nanostructured surfaces, Nanoscale Microscale Thermophys. Eng. 18 (2014) 223–250.

[6] F. Liu, G. Ghigliotti, J. Feng, C. Chen, Numerical simulations of self-propelled jumping upon drop coalescence on non-wetting surfaces, J. Fluid Mech. 752 (2014) 39–65.

[7] J. Wasserfall, P. Figueiredo, R. Kneer, W. Rohlfs, P. Pischke, Coalescence-induced droplet jumping on superhydrophobic surfaces: Effects of droplet mismatch, Phys. Rev. Fluids 2 (12) (2017) 123601.

[8] Y. Wang, P. Ming, Dynamic and energy analysis of coalescence-induced self-propelled jumping of binary unequal-sized droplets, Phys. Fluids 31 (12) (2019) 122108.

[9] C. Fuqiang, S. Li, Z. Ni, D. Wen, Departure velocity of rolling droplet jumping, Langmuir 36 (14) (2020) 3713–3719.

[10] S. Li, F. Chu, J. Zhang, D. Brutin, D. Wen, Droplet jumping induced by coalescence of a moving droplet and a static one: Effect of initial velocity, Chem. Eng. Sci. 211 (2020) 115252.

[11] K. Wang, Q. Liang, R. Jiang, Y. Zheng, Z. Lan, X. Ma, Self-enhancement of droplet jumping velocity: the interaction of liquid bridge and surface texture, RSC Adv. 6 (101) (2016) 99314–99321.

[12] Q. Peng, X. Yan, J. Li, L. Li, H. Cha, Y. Ding, C. Dang, L. Jia, N. Miljkovic, Breaking droplet jumping energy conversion limits with superhydrophobic microgrooves, Langmuir 36 (32) (2020) 9510–9522.

[13] Z. Yuan, Z. Hu, F. Chu, X. Wu, Enhanced and guided self-propelled jumping on the superhydrophobic surfaces with macrotexture, Appl. Phys. 115 (16) (2019) 163701.

[14] C. Lo, C. Wang, M. Lu, Scale effect on dropwise condensation on superhydrophobic surfaces, ACS Appl. Mater. Interfaces 6 (16) (2014) 14353–14359.

[15] M. Mulroe, B. Srijanto, S. Ahmadi, C. Collier, J. Boreyko, Tuning superhydrophobic nanostructures to enhance jumping-droplet condensation, ACS Appl. Mater. Interfaces 11 (8) (2017) 8499–8510.

[16] S. Farokhirad, J. Morris, T. Lee, Coalescence-induced jumping of droplet: Inertia and viscosity effects, Phys. Fluids 27 (10) (2015) 102102.

[17] H. Vahabi, W. Wang, S. Davies, J. Mabry, A. Kota, Coalescence-induced self-propulsion of droplets on superomniphobic surfaces, ACS Appl. Mater. Interfaces 9 (34) (2017) 29328–29336.

[18] X. Yan, L. Zhang, S. Sett, L. Feng, C. Zhao, Z. Huang, H. Vahabi, A. Kota, F. Chen, N. Miljkovic, Droplet jumping: effects of droplet size, surface structure, pinning, and liquid properties, ACS Nano 13 (2) (2019) 1309–1323.

[19] H. Cha, C. Xu, J. Sotelo, J. Chun, Y. Yokoyama, R. Enright, N. Miljkovic, Coalescence-induced nanodroplet jumping, Phys. Rev. Fluids 1 (6) (2016) 064102.

[20] P. Yue, J. Feng, Phase-field simulations of dynamic wetting of viscoelastic fluids, J. Non-Newton. Fluid Mech. 189 (2012) 8–13.

[21] Y. Wang, D. Minh, G. Amberg, Dynamic wetting of viscoelastic droplets, Phys. Rev. E 92 (4) (2015) 043002.

[22] Y. Wang, M. Do-Quang, G. Amberg, Impact of viscoelastic droplets, J. Non-Newton. Fluid Mech. 243 (2017) 38–46.

[23] P. Yue, J. Feng, C. Liu, J. Shen, Diffuse-interface simulations of drop coalescence and retraction in viscoelastic fluids, J. Non-Newton. Fluid Mech. 129 (3) (2005) 163–176.

[24] P. Yue, C. Zhou, J. Feng, A computational study of the coalescence between a drop and an interface in Newtonian and viscoelastic fluids, Phys. Fluids 18 (10) (2006) 102102.

[25] P. Dekker, M. Hack, W. Tewes, C. Datt, A. Bouillant, J. Snoeijer, When elasticity affects drop coalescence, Phys. Rev. Lett. 128 (2) (2022) 028004.

[26] K. Bazesefidpar, L. Brandt, O. Tammisola, A dual resolution phase-field solver for wetting of viscoelastic droplets, Internat. J. Numer. Methods Fluids (2022) 1–25, http://dx.doi.org/10.1002/fld.5100.

[27] P. Yue, J. Feng, C. Liu, J. Shen, A diffuse-interface method for simulating two-phase flows of complex fluids, J. Fluid Mech. 515 (2004) 293–317.

[28] H. Abels, H. Garcke, G. Grün, Thermodynamically consistent, frame indifferent diffuse interface models for incompressible two-phase flows with different densities, Math. Models Methods Appl. Sci. 22 (03) (2012) 1150013.

[29] D. Jacqmin, Contact-line dynamics of a diffuse fluid interface, J. Fluid Mech. 402 (2000) 57–88.

[30] T. Qian, X. Wang, P. Sheng, Molecular scale contact line hydrodynamics of immiscible flows, Phys. Rev. E 68 (1) (2003) 016306.

[31] S. Dong, On imposing dynamic contact-angle boundary conditions for wall-bounded liquid–gas flows, Comput. Methods Appl. Mech. Engrg. 247 (2012) 179–200.

[32] R. Fattal, R. Kupferman, Constitutive laws for the matrix-logarithm of the conformation tensor, J. Non-Newton. Fluid Mech. 123 (2-3) (2004) 281–285.

[33] R. Fattal, R. Kupferman, Time-dependent simulation of viscoelastic flows at high weissenberg number using the log-conformation representation, J. Non-Newton. Fluid Mech. 126 (1) (2005) 23–37.

[34] S. Gottlieb, C. Shu, Total variation diminishing runge-kutta schemes, Math. Comp. 67 (221) (1998) 73–85.

[35] R. Borges, M. Carmona, B. Costa, W. Don, An improved weighted essentially non-oscillatory scheme for hyperbolic conservation laws, J. Comput. Phys. 227 (6) (2008) 3191–3211.

[36] S. Boyaval, T. Lelièvre, C. Mangoubi, Free-energy-dissipative schemes for the oldroyd-b model, ESAIM: Math. Model. Numer. Anal. Modél. Math. Anal. Numér. 43 (3) (2009) 523–561.

[37] D. Mokbel, H. Abels, S. Aland, A phase-field model for fluid–structure interaction, J. Comput. Phys. 372 (2018) 823–840.

[38] F. Magaletti, F. Picano, M. Chinappi, L. Marino, C. Casciola, The sharp-interface limit of the Cahn-Hilliard/Navier-Stokes model for binary fluids, J. Fluid Mech. 714 (2013) 95–126.

[39] X. Xu, Y. Di, H. Yu, Sharp-interface limits of a phase-field model with a generalized Navier slip boundary condition for moving contact lines, J. Fluid Mech. 849 (2018) 805–833.

[40] P. Yue, C. Zhou, J. Feng, Sharp-interface limit of the cahn–hilliard model for moving contact lines, J. Fluid Mech. 645 (2010) 279–294.

[41] Y. Cheng, J. Xu, Y. Sui, Numerical investigation of coalescence-induced droplet jumping on superhydrophobic surfaces for efficient dropwise condensation heat transfer, Int. J. Heat Mass Transfer 95 (2018) 506–516.

[42] D. Khismatullin, A. Nadim, Shape oscillations of a viscoelastic drop, Phys. Rev. E 63 (6) (2001) 061508.

[43] G. Amberg, Detailed modelling of contact line motion in oscillatory wetting, NPJ Microgr. 8 (1) (2022) 1–8.

[44] H. Xu, A. Clarke, J. Rothstein, R. Poole, Viscoelastic drops moving on hydrophilic and superhydrophobic surfaces, J. Colloid Interface Sci. 513 (2018) 53–61.

[45] P. Yue, Thermodynamically consistent phase-field modelling of contact angle hysteresis, J. Fluid Mech. 899 (2020) A15.